CSIRO PUBLISHING

Marine and Freshwater Research, 2007, **58**, 966–981 www.publish.csiro.au/journals/mfr

The effect of packaging of chlorophyll within phytoplankton and light scattering in a coupled physical–biological ocean model

Mark E. Baird[A,B], *Patrick G. Timko*[A] *and Lujia Wu*[A]

[A]Climate Change Research Centre, School of Mathematics and Statistics, University of New South Wales, Sydney, NSW 2052, Australia.
[B]Corresponding author. Email: m.baird@unsw.edu.au

Abstract. A coupled physical–biological model forced with spectrally resolved solar radiation is used to investigate the effect of packaging of pigment and light scattering on physical and biological properties in the open ocean. Simulations are undertaken with three alternate formulations of vertical attenuation, which consider: (1) chlorophyll as dissolved in the water column; (2) chlorophyll packaged into phytoplankton cells with no scattering; and (3) packaged chlorophyll with scattering. In the coupled model, depth-resolved solar heating depends on the vertical profile of phytoplankton concentration, creating a feedback mechanism between the physical and biological states.

The particular scenario investigated is a northerly wind off the coast of south-east Australia. The packaging of chlorophyll approximately halves the attenuation rate of 340–500 nm light and a phytoplankton maximum forms ~10 m deeper than in the dissolved chlorophyll case, with a corresponding adjustment of the dissolved inorganic nitrogen and zooplankton fields. Scattering approximately doubles the vertical attenuation of 340–600 nm light, lifting the phytoplankton maximum by ~10 m when compared with the packaged chlorophyll case. Additionally, strong horizontal gradients in chlorophyll distribution associated with filaments of upwelled water inshore of the East Australian Current, when modelled with alternate formulations of vertical light attenuation, result in circulation changes. The explicit representation of the packaging of pigment and light scattering is worth considering in coupled physical–biological modelling studies.

Additional keywords: biological induced heating, East Australian Current, light scattering, package effect, Port Stephens.

Introduction

The rate at which light is attenuated in aquatic environments affects the vertical distribution of solar heating (Lewis *et al*. 1983) and primary production (Kirk 1994). The combination of the two factors provides a feedback mechanism between the physical and biological states of an aquatic ecosystem (Stramska and Dickey 1993; Edwards *et al*. 2001; Oschlies 2004; Gildor and Naik 2005).

The attenuation of light is a combination of absorption and scattering processes. A range of models have been used to consider light attenuation in the ocean. Simple models include those that do not explicitly distinguish between absorption and scattering and are often used in pelagic ecosystem models (Fasham *et al*. 1990). More complex models consider both absorption and scattering (Morel 1988; Sathyendranath *et al*. 1989) and/or consider a spectrally resolved light field (Gregg and Carder 1990). More sophisticated models still, commonly used for modelling radiation in the atmosphere, are based on electromagnetic theories (Mishchenko *et al*. 2002).

The absorption of light by phytoplankton is a function of the shape, size and optical properties of the cell (Kirk 1994). The packaging of pigments within cells, called the package effect, reduces light attenuation when compared with the same quantity of pigment dissolved in the water column (Duyens 1956). The simplest physically based consideration of these phenomena can be undertaken using ray-tracing techniques or geometric optics (Kirk 1975, 1976). As well as reducing the attenuation coefficient, the package effect also flattens the absorption spectrum (Duyens 1956). That is, the package effect results in a greater reduction in attenuation at wavelengths that are strongly absorbed.

Scattering increases the attenuation of light through a combination of reflection and diffraction. The process of scattering is generally more complicated to model than absorption. Sophisticated models include the consideration of both the intensity and direction of scattered light. These more elaborate scattering calculations are computationally expensive (Mishchenko *et al*. 2002). For the case of scattering by clear water and phytoplankton in the open ocean, empirical relationships (Kirk 1981, 1991) have been found to be sufficiently accurate to quantify the effects of scattering on the vertical attenuation of light, and will be used in this study.

Several studies have investigated the feedback between physical and biological states in marine systems. Edwards *et al*. (2001) undertook analytical calculations that showed a tight horizontal gradient in chlorophyll can produce vertical velocities of up to

 10.1071/MF07055 1323-1650/07/100966

0.2 mm s^{-1}, and along front velocities of ~2 cm s^{-1}. In further work, Edwards *et al*. (2004) derived the vertical circulation cells that develop below a filament of high chlorophyll water. Further work on the feedback between physical and biological states has considered the effect of vertical mixing on ocean basin scales (Oschlies 2004). Each of these studies used a simple model of vertical attenuation that did not distinguish between absorption and scattering, and did not include the differences in optical properties across the spectrum of solar radiation.

This paper investigates the effects of using three alternate formulations of vertical light attenuation in a three-dimensional coupled physical–biological model with spectrally resolved solar radiation forcing. The formulations are based on: (1) chlorophyll dissolved in the water column; (2) chlorophyll packaged within cells with no scattering; and (3) chlorophyll packaged within cells with scattering. In particular, numerical experiments are designed to separate the effects of the packaging of pigments within cells and scattering on properties of the physical and biological systems.

The physical–biological model used in this study is a configuration of the Princeton Ocean Model for the waters off south-east Australia during upwelling-favourable northerly winds, representative of a strong western boundary current in oligotrophic waters with an upwelling-driven coastal phytoplankton bloom. The study area is near a well known upwelling site off Port Stephens, south-east Australia (Oke and Middleton 2001) (Fig. 1). At this location, the bottom friction associated with the East Australia Current (EAC) drives on-shore transport in the bottom boundary layer bringing nutrient-rich dense water onto the continental shelf (Roughan and Middleton 2002). Upwelling-favourable winds can lift these nutrient-rich waters to the surface, where they are entrained into the southward flow of the EAC. Under these conditions, filaments of high chlorophyll can form, with a width of ~10 km (see MODIS satellite image of Fig. 1 in Baird *et al*. 2006*a*).

A new <6 km resolution configuration of the Princeton Ocean Model for the waters off south-east Australia produces filaments of upwelled water of a similar dimension to observations. Coupled to a simple biological model, filaments of upwelled water develop high phytoplankton biomass. The filament of high phytoplankton biomass produced provides a strong horizontal gradient in absorption and scattering properties. This gradient in optical properties provides a good scenario to investigate the effects of alternate formulations of vertical attenuation and the feedback between the physical and biological properties.

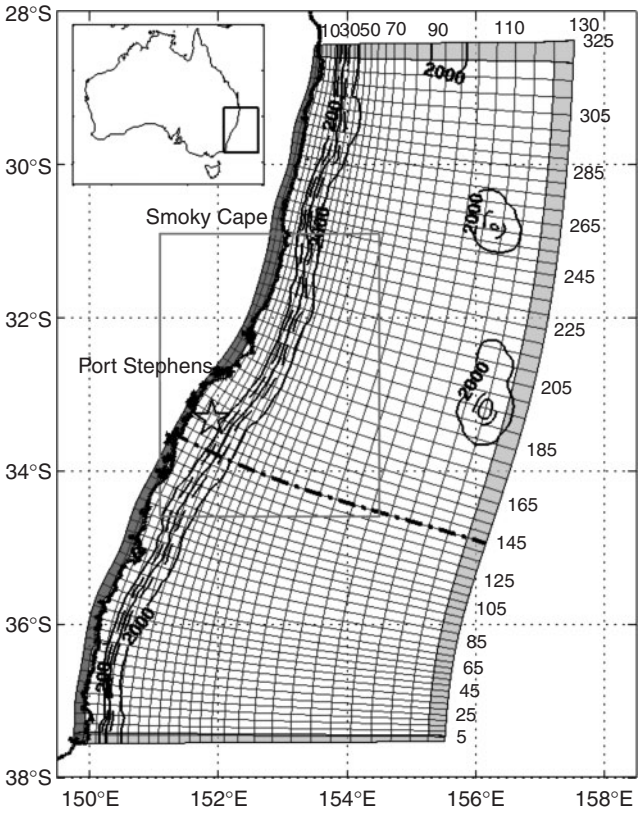

Fig. 1. The model grid. Insert at top left shows map location on the east coast of Australia. The first grid line, and then every 5th grid line in the *x* (approx. E–W) and *y* (approx. N–S) directions are shown. The heavily shaded region on the coastal boundary is the portion of the grid that is land. The thick line shows the Australian coastline. The lightly shaded regions on the northern, eastern and southern boundaries are regions of the grid on which boundary conditions are applied. Line contours show isobaths of 200, 1000 and 2000 m, and dashed contours show 500 and 1500 m. The grey boxed region is the domain for Figs 7, 9, 10, 11. The dot-dash line along y-slice 145 is used in Figs 5, 6, 11. A star shows the location that vertical profiles of the light spectrum are displayed in Fig. 4.

Physical model

The physical model is the Princeton Ocean Model (POM), which has a free surface and solves the non-linear primitive equations on a horizontal orthogonal curvilinear grid and a vertical sigma (terrain following) coordinate system using finite difference methods (Blumberg and Mellor 1987). The Craig–Banner scheme (Craig and Banner 1994) for calculating the wave-driven flux of turbulent kinetic energy at the surface has been implemented. A hydrostatic correction term for sigma-coordinate models has also been included (Chu and Fan 2003).

The physical configuration (Fig. 1) extends along the NSW coast from 28.4°S to 37.5°S, a distance of 1025 km, and extends offshore between 395 km (at 28.4°S) and 500 km (at 37.5°S). The grid has 130 grid points in the offshore direction with a resolution between 1 and 6 km, and 325 points in the along-shore direction with a resolution between 1.5 and 6 km. In the region studied in this paper (grey boxed area in Fig. 1), offshore resolution is between 1 and 3 km, and the along-shore resolution between 3 and 5 km. The outer six boxes on the northern, eastern and southern boundaries have smoothed topographies and are used to implement the boundary conditions. The interior of the model domain consists of points 1–124 in the offshore direction and 7–319 in the alongshore direction.

The vertical sigma coordinates contains 31 layers, with greater resolution in the top and bottom boundary layers. The minimum and maximum depths are set to 50 and 2000 m respectively. The physical model solves the external (barotropic) mode with a 1.7-s timestep and the internal (baroclinic) mode with a 60-s timestep.

A diagnostic variable ideal age (England 1995; Hall and Haine 2002) is used to track the transport of nutrient-rich bottom waters into the euphotic zone. The dynamics of ideal age, τ, are described by:

$$\frac{\partial \tau}{\partial t} + v \cdot \nabla \tau = \nabla \cdot (K \nabla \tau) + \Theta(z) \quad (1)$$

where Θ ($z < 90$ m depth) $= 1$, Θ ($z > 90$ m depth) $= 0$, the symbol $\nabla = \left(\frac{\partial}{\partial x}, \frac{\partial}{\partial y}, \frac{\partial}{\partial z}\right)$, v is the velocity field, K is the eddy diffusion coefficient which varies in space and time. The term Θ increments the value of τ by one day every day for water above 90 m. Ideal age in this application is the average time parcels of water within a volume have been above the 90 m depth level since the beginning of the simulation and is subject to mixing and advective processes.

Light model

The light intensity at wavelength λ at the bottom of a layer dz thick, $I_{\lambda,bot}$, is given by:

$$I_{\lambda,bot} = I_{\lambda,top} e^{-K_\lambda dz} \quad (2)$$

where $I_{\lambda,top}$ is the light intensity at wavelength λ at the top of the layer and K_λ is the vertical attenuation coefficient at wavelength λ, a result of both absorption and scattering processes. The average light intensity within the layer at wavelength λ, I_λ, is given by:

$$I_\lambda = \frac{I_{\lambda,top} - I_{\lambda,bot}}{K_\lambda dz} \quad (3)$$

In this paper, the attenuation coefficient, K_λ, is calculated three ways.

(1) *Chlorophyll dissolved in the water column*. The concentration of chlorophyll in the water column is equal to the intracellular concentration of chlorophyll, C, multiplied by the volume of the cell, V, and the concentration of cells, n. The vertical attenuation coefficient at wavelength λ calculated when considering chlorophyll dissolved in the water column, $K_{\lambda,c}$, is given by:

$$K_{\lambda,c} = \frac{k_\lambda + \gamma_\lambda nCV}{\cos\theta} \quad (4)$$

where k_λ is the absorption coefficient of clear water (Fig. 2*c*), γ_λ is the chlorophyll-specific absorption coefficient (Fig. 2*d*) and the concentration of cells, n, is given by $P/m_{P,N}$ (see biological model description). The term $\cos\theta$, accounts for the zenith angle, θ, at which light travels through the water column.

(2) *Chlorophyll packaged in phytoplankton, with no scattering*. The packaging of chlorophyll withinphytoplankton cells reduces the attenuation coefficient. To include this effect, the absorption cross section of a phytoplankton cell is calculated. In this paper, the absorption cross section is calculated using geometric optics (Kirk 1994) assuming that phytoplankton cells are spherical with a homogeneous concentration of pigment and no internal scattering. By assuming a homogeneous spherical cell, cell orientation has no influence. The absorption cross section varies between 0 (of a non-absorbing cell) and πr^2 (the projected area of the cell).

The analytical solution of the absorption cross section for a sphere of radius r is given by (Kirk 1975):

$$\overline{aA_\lambda} = \pi r^2 \left(1 - \frac{2(1 - (1 + 2\gamma_\lambda Cr)e^{-2\gamma_\lambda Cr})}{(2\gamma_\lambda Cr)^2}\right) \quad (5)$$

where A is the cross-sectional area perpendicular to the light or the projected area, and is a function of orientation, and a is the fraction of light absorbed for a particular pencil of light through the sphere. The fraction a is a function of the chlorophyll-specific absorption coefficient, γ_λ (Fig. 2*d*), pigment concentration, C, orientation and the distance between entry and exit points (Baird 2003). The bar over $\overline{aA_\lambda}$ signifies the integral over a random orientation of the product of A and a. The value of $\overline{aA_\lambda}$ is an approximation using geometric optics of the absorption cross section which when determined experimentally is typically given the symbol α. Only the calculated absorption cross section (Fig. 2*f*) is used in this paper so the notation $\overline{aA_\lambda}$ is used throughout.

The attenuation coefficient when considering chlorophyll packaged within cells, $K_{\lambda,p}$, is given by:

$$K_{\lambda,p} = \frac{k_\lambda + n\overline{aA_\lambda}}{\cos\theta} \quad (6)$$

(3) *Chlorophyll packaged in phytoplankton, with scattering*. The effect of scattering on vertical attenuation is quantified using an empirical relationship between observation of attenuation coefficients and absorption and scattering properties (Kirk 1991). The relationship represents scattering as a fractional increase in length of travel of light between two depths when compared with that of the non-scattering case. The vertical attenuation coefficient when considering absorption of chlorophyll packaged within cells and scattering, $K_{\lambda,p\&s}$ is given by:

$$K_{\lambda,p\&s} = \frac{k_\lambda + n\overline{aA_\lambda}}{\cos\theta}\sqrt{1 + (g_1 + g_2\cos\theta)\frac{b_{T,\lambda}}{k_\lambda + n\overline{aA_\lambda}}} \quad (7)$$

where g_1 and g_2 are empirical constants and take values of 0.30 and 0.14 respectively (based on offshore, southern California values in Kirk (1991)). The total scattering coefficient, $b_{T,\lambda} = b_{w,\lambda} + b_{phy,\lambda} nCV$, is the sum of scattering due to clear water, $b_{w,\lambda}$ (Fig. 2*e*), and the product of the chlorophyll-specific phytoplankton scattering coefficient, $b_{phy,\lambda}$, and the water column chlorophyll concentration, nCV. A typical value for marine phytoplankton of $b_{phy,\lambda} = 0.2$ (mg Chl a m^{-2})$^{-1}$ is used for all wavelengths (Kirk 1994).

The energy absorbed at depth z gives rise to a local increase in temperature, T (Lewis *et al.* 1983). Assuming all energy absorbed is dissipated immediately as heat, the local rate of change of T is given by:

$$\frac{\partial T}{\partial t} = -\frac{1}{\rho c_p}\int \frac{\partial I}{\partial z}\, d\lambda \quad (8)$$

where the product of density and heat capacity, ρc_p, is assumed to be constant (4.1876×10^6 J m^{-3} K^{-1}). A small fraction of the light absorbed, less than 2% of visible light, becomes energy stored in organic molecules (Morel 1988), and is dissipated as

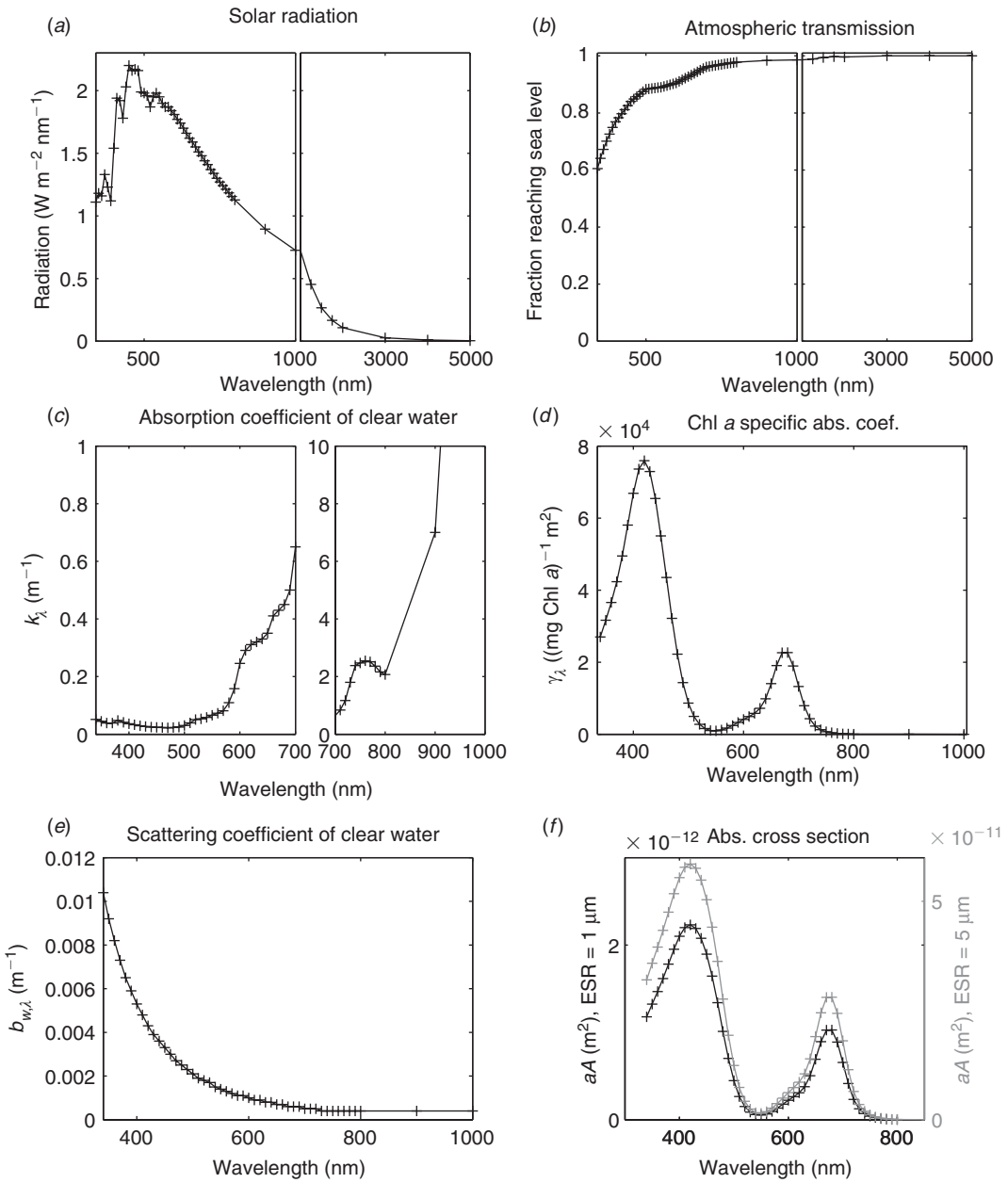

Fig. 2. The spectrally resolved optical properties: (*a*) wavelength-resolved solar radiation above the Earth's atmosphere (Koller 1965); (*b*) transmission coefficient through a cloudless sky at the zenith sun (Koller 1965); (*c*) attenuation coefficient of clear water, k_λ (Kirk 1994); (*d*) chlorophyll a specific absorbance coefficient, γ_λ (Hoepffner and Sathyendranath 1991); (*e*) scattering coefficient of clear water $b_{w,\lambda}$ (Smith and Baker 1981; Pegau *et al*. 2003); (*f*) absorption cross section of a 1 µm and 5 µm spherical phytoplankton cell based on Eqns 5, 17, 18.

heat at a later time. The delayed dissipation of this negligible fraction is not considered in this study.

The solar radiation intensity at the edge of the Earth's atmosphere is shown in Fig. 2*a*. In the simulations, solar radiation is assumed to be composed of 57 discrete wavelengths (crosses in Fig. 2). The intensity at each discrete wavelength is the integral of the radiation from the midpoints between bands. The wavelengths used are 340, 350, . . . , 790, 800, 900, 1000, 1250, 1500, 1750, 2000, 3000, 4000, 5000 and 6000 nm. The spectral grid is most resolved in the photosynthetically available wavelengths at which attenuation properties are highly variable, and less resolved in the infrared where attenuation properties vary in a smoother manner.

The solar radiation at the sea surface, and the zenith angle, θ, have been calculated using orbital cycles (Brock 1981) and a wavelength-dependent atmospheric transmission coefficient

(Fig. 2*b*). The surface albedo as a function of zenith angle is calculated using Fresnel's equation (Kirk 1994). Snell's law is used to account for the refraction of light at the air–water interface (Kirk 1994). In order to exclude a seasonal signal and the small latitudinal variation, the whole model domain is forced with a solar radiation flux for January 1 at 34°S each model day. The flux is calculated every 1 min of model time. A factor of 0.8 reduction has been applied equally over all wavelengths to account for the mean observed difference between clear sky solar radiation and the downward solar radiation flux for the study region during the austral summer (as determined from NCEP reanalysis: Kistler *et al*. 2001). To avoid complication of the analysis due to a drift in ocean-heat content, a surface heat loss equal to the solar radiation flux at the surface is applied.

Biological model

The biological model used is the pelagic ecosystem model of Baird *et al*. (2004). The model contains five state variables: dissolved inorganic nitrogen, or DIN (N), phytoplankton (P), zooplankton (Z) and phytoplankton reserves of nitrogen (R_N) and energy (R_I). The model includes the process of nutrient uptake and light capture by phytoplankton, phytoplankton growth from internal reserves, zooplankton grazing on phytoplankton and the mortality and sinking of both phytoplankton and zooplankton. Where possible, physical descriptions of the limits to ecological processes have been used. For example, the description of grazing rates of zooplankton on phytoplankton incorporates an encounter-rate calculation, based on the encounter rates of particles in a turbulent fluid, which places a maximum rate on zooplankton ingestion. The physical limits are used up until a physiological rate, such as maximum growth rate, becomes more limiting.

The coupling of the physical and biological models results in an advection–diffusion-reaction (ADR) equation for phytoplankton biomass with the following dynamical terms:

$$\overbrace{\frac{\partial P}{\partial t}}^{\text{tendency}} \underbrace{+ v\cdot\nabla P}_{\text{advection}} = \overbrace{\nabla\cdot(K\nabla P)}^{\text{diffusion}} \underbrace{+ F_P}_{\text{biological terms}} \overbrace{- w_P\frac{\partial P}{\partial z}}^{\text{sinking}} \quad (9)$$

where the symbol $\nabla = \left(\frac{\partial}{\partial x}, \frac{\partial}{\partial y}, \frac{\partial}{\partial z}\right)$, v is the velocity field, K is the eddy diffusion coefficient, and varies in space and time, F_P is the sink/source of phytoplankton due to biological processes and w_P is the sinking velocity of phytoplankton. The ADR equations for DIN, zooplankton and reserves of nitrogen and energy are given in a two-dimensional form in equations 12–16 of Baird *et al*. (2004), and can be extended to three dimensions following Eqn 9. Note that although these equations are written in a z-coordinate system, they are solved in the sigma coordinates of the Princeton Ocean Model.

The equations for the sink/sources of change of DIN, phytoplankton, zooplankton, nitrogen and energy reserves are given by:

$$F_N = \underbrace{k_N\left(\frac{R_N^{max}-R_N}{R_N^{max}}\right)\frac{P}{m_{P,N}}}_{\text{DIN uptake}} + \underbrace{\zeta_P P + \zeta_P R_N\frac{P}{m_{P,N}} + \zeta_Z Z}_{\text{regeneration (owing to mortality)}} + \gamma\min\left[\phi P/m_{P,N}, \frac{\mu_Z^{max}}{(1-\gamma)}\right]Z + \underbrace{\min\left[\phi P/m_{P,N}, \frac{\mu_Z^{max}}{(1-\gamma)}\right]Z\frac{R_N}{m_{P,N}}}_{\text{regeneration (owing to sloppy grazing)}} \quad (10)$$

$$F_{R_N} = \underbrace{+k_N\left(\frac{R_N^{max}-R_N}{R_N^{max}}\right)}_{\text{DIN uptake}} \underbrace{-\mu_P^{max}(m_{P,N}+R_N)\frac{R_N}{R_N^{max}}\frac{R_I}{R_I^{max}}}_{\text{phytoplankton growth}} \quad (11)$$

$$F_{R_I} = \underbrace{+k_I\left(\frac{R_I^{max}-R_I}{R_I^{max}}\right)}_{\text{light capture}} \underbrace{-\mu_P^{max}(m_{P,I}+R_I)\frac{R_N}{R_N^{max}}\frac{R_I}{R_I^{max}}}_{\text{phytoplankton growth}} \quad (12)$$

$$F_P = \underbrace{\mu_P^{max}\frac{R_N}{R_N^{max}}\frac{R_I}{R_I^{max}}P}_{\text{phytoplankton growth}} \underbrace{-\min\left[\phi P/m_{P,N}, \frac{\mu_Z^{max}}{1-\gamma}\right]Z}_{\text{grazing}} \underbrace{-\zeta_P P}_{\text{mortality}} \quad (13)$$

$$F_Z = \underbrace{+\min\left[\phi P/m_{P,N}, \frac{\mu_Z^{max}}{1-\gamma}\right]Z - \gamma\min\left[\phi P/m_{P,N}, \frac{\mu_Z^{max}}{1-\gamma}\right]Z}_{\text{zooplankton growth}} \underbrace{-\zeta_Z Z}_{\text{mortality}} \quad (14)$$

where k_N and k_I are the maximum rates of DIN and energy uptake of phytoplankton respectively (and are a function of N and incident light respectively), R_N^{max} and R_I^{max} are the maximum values of R_N and R_I respectively, μ_P^{max} and μ_Z^{max} are the maximum growth rates of phytoplankton and zooplankton respectively, ϕ is the encounter rate coefficient between phytoplankton and zooplankton, ζ_P and ζ_Z are the linear mortality rates of phytoplankton and zooplankton respectively and $(1-\gamma)$ is the assimilation efficiency of grazing. The sink/source terms F_N, F_P and F_Z have units of mol N m^{-3} s^{-1}, whereas F_{R_I} has units of mol N cell^{-1} s^{-1}, and F_{R_I} has units of mol photon cell^{-1} s^{-1}. The term $P/m_{P,N}$, which appears in the DIN uptake and the phytoplankton grazing terms, is the concentration of phytoplankton cells.

Phytoplankton incorporate inorganic carbon into organic molecules during photosynthesis. Energy reserves represent this fixed carbon, before it is combined with nitrogen. The increase in phytoplankton energy reserves depends on the number of photons absorbed independent of the energy of the photon. The energy of one photon is given by hc/λ', where $c = 2.998\times10^8$ m s^{-1} is the speed of light, $h = 6.626\times10^{34}$ J s^{-1} is the Planck constant and λ' is the wavelength (m) (Atkins 1994). Rearranging, and using nanometre as

Table 1. Parameter values used in the simulations for a 1 μm and 5 μm radius phytoplankton cell, and 20 μm radius zooplankton cell

Wavelength-dependent parameter values are given in Fig. 2

Parameter	Symbol	$r_P = 1\,\mu m$	$r_P = 5\,\mu m$	Units
Z radius	r_Z	20	20	μm
Assimilation coefficient	γ	0.3	0.3	–
P mortality	ζ_P	0.0	0.0	day^{-1}
Z mortality	ζ_Z	0.2	0.2	day^{-1}
Parameters calculated from r_P and r_Z				
P nitrogen content	$m_{P,N}$	1.34×10^{-14}	5.21×10^{-13}	mol N $cell^{-1}$
P energy content	$m_{P,I}$	8.87×10^{-13}	3.45×10^{-11}	mol I $cell^{-1}$
Max. P N reserves	R_N^{max}	1.34×10^{-14}	5.21×10^{-13}	mol N $cell^{-1}$
Max. P energy reserves	R_I^{max}	8.87×10^{-13}	3.45×10^{-11}	mol I $cell^{-1}$
Z nitrogen content	$m_{Z,N}$	1.22×10^{-11}	1.22×10^{-11}	mol N $cell^{-1}$
Diffusion shape factor	ψ	1.26×10^{-5}	6.28×10^{-5}	m $cell^{-1}$
P Chl concentration	C	1.35×10^{7}	3.01×10^{6}	mg Chl m^{-3}
P Chl:N ratio	CV/m_N	4.21	3.03	mg Chl *a* (mmol N)$^{-1}$
Max. growth rate of P	μ_P^{max}	2.82	2.00	day^{-1}
Max. growth rate of Z	μ_Z^{max}	1.40	1.40	day^{-1}
Max. sinking rate of P	w_P	0.0448	0.2943	m day^{-1}
Max. sinking rate of Z	w_Z	0.0	0.0	m day^{-1}
Relative encounter velocity	U	310	310	μm s^{-1}
Pigment spectrum scatter coefficient	b_{phy}	0.2	0.2	m^2 (mg Chl *a*)$^{-1}$
θ independent scatter coefficient	g_1	0.30	0.30	–
θ dependent scatter coefficient	g_2	0.14	0.14	–
Cloud fraction	–	0.8	0.8	–

the units of wavelength ($1\,nm = 10^{-9}$ m), conversion between an amount of energy absorbed at wavelength, λ (nm), and the number of photons absorbed is given by:

$$1 \text{ photon} = 5.03 \times 10^{15} \lambda / A_V \text{ Joule} \quad (15)$$

where $A_V = 6.02 \times 10^{23}$ mol^{-1} is the Avagadro constant (Atkins 1994). The maximum rate of energy uptake, k_I (mol photon $cell^{-1}$ s^{-1}), is equivalent to the instantaneous rate of photosynthesis in a low-light environment, and is given by:

$$k_I = \frac{5.03 \times 10^{15}}{A_V} \int I \overline{a A_\lambda} \lambda d\lambda \quad (16)$$

The combination of energy reserves and nitrogen reserves to create phytoplankton organic matter is based on a fixed C:N stoichiometry. The calculation of $m_{P,I}$, the stoichiometry coefficient of energy, is based on the quantum yield of photosynthesis and the Redfield ratio (C:N = 106:16: Redfield *et al*. 1963). The theoretical maximum quantum yield is 0.125 mol C (mol photon)$^{-1}$. A more realistic value of 0.1 mol C (mol photon)$^{-1}$ has been used (Kirk 1994).

A more detailed description of the biological model can be found in Baird *et al*. (2004), and its application to the waters off south-east Australia in Baird *et al*. (2006*a*) and Baird *et al*. (2006*b*). In particular, the calculation of k_N, k_I and ϕ in terms of properties of the individual cells and environmental conditions can be found in Baird *et al*. (2004).

The parameters describing phytoplankton are given in Table 1. The allometric relationship used to calculate the chlorophyll concentration of a cell is given by (Finkel 2001):

$$C = 2.06 \times 10^7 (10^{18} V)^{-0.320} \text{ mg Chl } a \text{ m}^{-3} \quad (17)$$

where V is the volume of the phytoplankton cell (m^3). The allometric relationship for nitrogen as a function of cell volume is given by (Hofmann *et al*. 2000):

$$m_{P,N} = (16/106) 1.32 V^{0.758} \text{ mol N cell}^{-1} \quad (18)$$

Simulation details

Physical details

The initial temperature field is interpolated from sea surface temperature data and temperature at 250-m depth from January 1997 (Oke and Middleton 2001). Initial velocities are calculated using the thermal wind equations (fig. 3 in Baird *et al*. 2006*a*). The model is allowed to spin up for 2 days to ensure the internal velocity field has time to adjust before temperature and salinity are permitted to evolve. Along the southern and eastern boundaries a radiation boundary condition with relaxation is used, which permits oblique waves to radiate outwards (Marchesiello *et al*. 2001). At the northern boundary, the southward velocity is specified from the initial velocity estimated from the thermal wind equations and held constant. The western boundary, the south-east Australian coast, is a closed boundary.

The simulations are forced with a 0.1 N m^{-2} northerly (alongshore from the north) wind stress, ramped linearly from zero to 0.1 N m^{-2} over one day, and which remains constant for the rest of the simulation. The stress is tapered over the last six grid points to zero on the open boundaries. A wind stress of 0.1 N m^{-2} corresponds to a wind of ~5 m s^{-1}. After a further day of spin-up

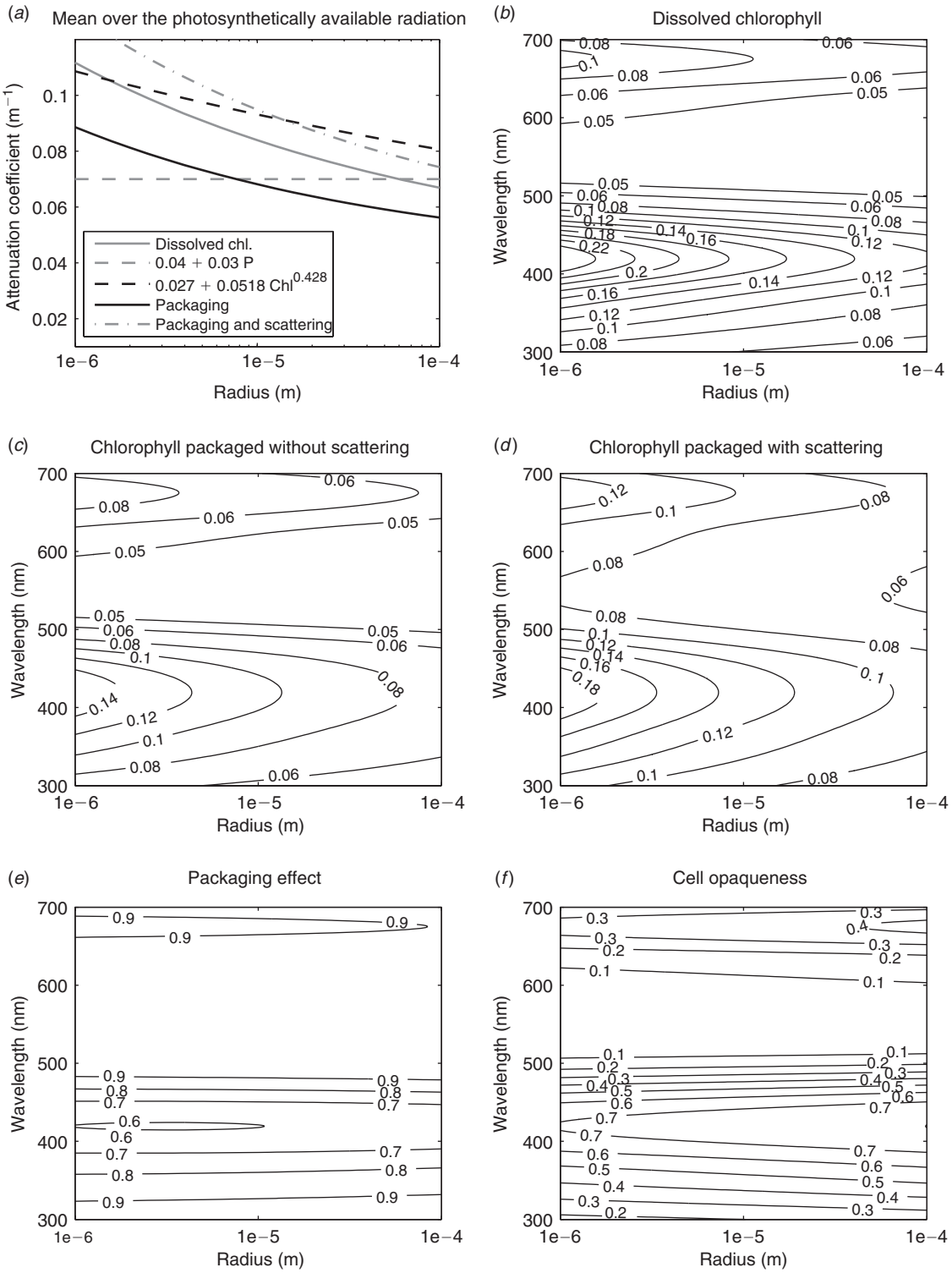

Fig. 3. The light attenuation coefficient, K, for a phytoplankton biomass of 1 mmol N m^{-3} (*a*) using five different formulations as a function of cell radii over the mean between 300 and 700 nm (the linear attenuation coefficient calculation takes a typical value of $k_c = 0.03$ m^2 (mmol N)$^{-1}$ (Fasham *et al*. 1990), whereas the non-linear form comes is based on Morel (1988)); (*b*) as a function of cell radii and wavelength for the dissolved chlorophyll case; (*c*) as a function of cell radii and wavelength for the packaged chlorophyll case without scattering; and (*d*) as a function of cell radii and wavelength for the packaged chlorophyll case with scattering. Panel (*e*) shows the package effect, $\overline{naA_\lambda}/(\gamma_\lambda nCV)$ and (*f*) cell opaqueness, $\overline{aA_\lambda}/(\pi r^2)$ based on spherical cells with a chlorophyll concentration to cell size relationship given by Finkel (2001) and the nitrogen to cell size relationship of Hofmann *et al*. (2000).

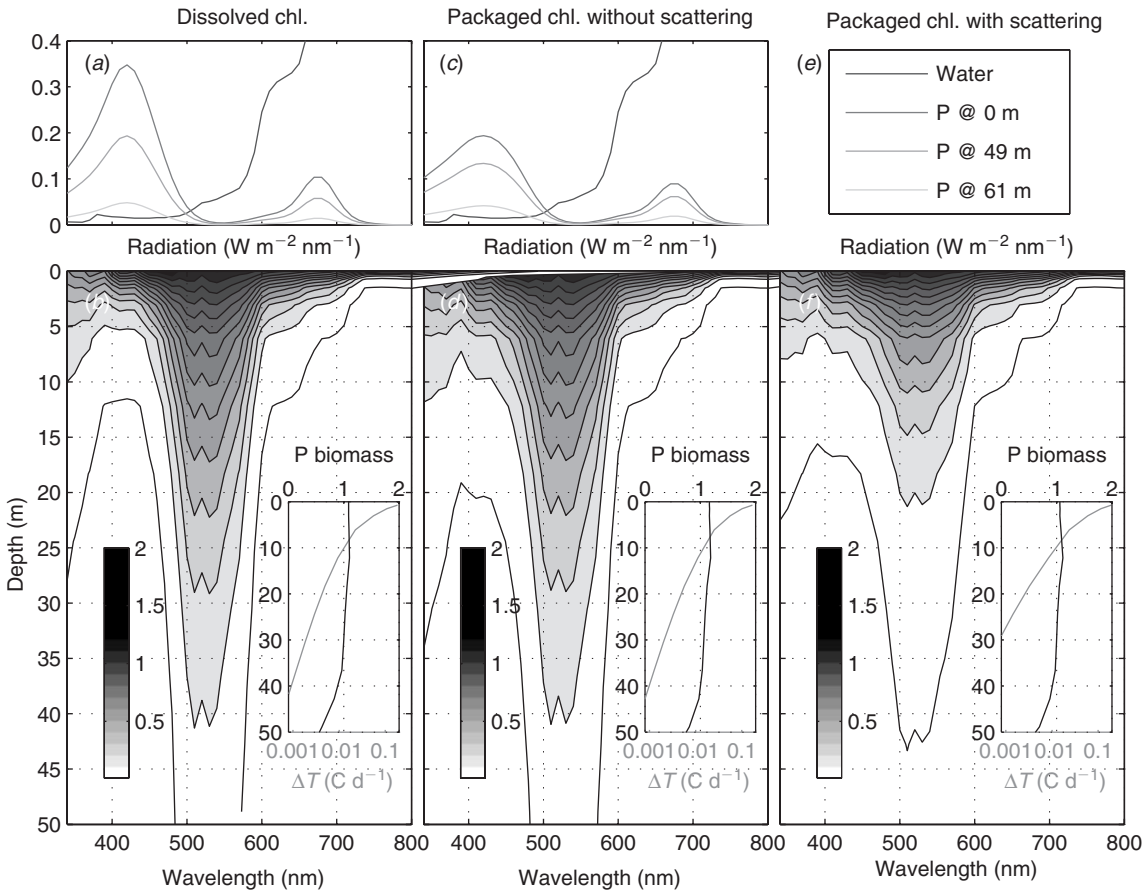

Fig. 4. Vertical profile of the light spectrum off Port Stephens (33°04′S 151°55′E, Fig. 1) on Day 20.5 for the dissolved chlorophyll (left), packaged chlorophyll (centre) and packaged and scattering (right) formulations of vertical attenuation. (*a*) and (*c*) are the absorbing components, (*b*), (*d*) and (*f*) are the spectrally resolved light field. The insert in Panels (*b*), (*d*) and (*f*) show the vertical profile of phytoplankton biomass (mmol N m^{-3}) on a linear scale and the local change in temperature due to solar heating on a $\log_{10}$ scale.

of the velocities, temperature and salinity are dynamically calculated. Model time begins after these 2 days of spin-up. The temperature and salinity fields undergo an adjustment during the formation of a bottom boundary layer along the shelf break on a time-scale of ∼1.5 days. To prevent unrealistic mixing during this adjustment phase, all biological state variables are held constant for further 2 days. Age begins varying at the same time as the biological variables, and so has a zero value at Day 2.0 throughout the domain. More details can be found in Baird *et al*. (2006*a*).

Biological details

Initial conditions were determined using a long-duration spin-up of the coupled model in a two-dimensional grid with zero-mean oscillating alongshore wind stress. The wind stress sets up a realistic profile of vertical diffusivity forming a surface mixed layer. By oscillating between an upwelling- and downwelling-favourable wind stress, no net upwelling occurs. The two-dimensional model is run for 375 days, at which stage the time derivatives of the biological fields are small. The output from the two-dimensional grid after 375 days can be viewed as a quasi steady-state response to idealised vertical mixing.

The biological boundary conditions at the surface, bottom and coast (western boundary) are zero flux. The open boundaries (north, south and east) have the same radiation condition as the physical variables and are relaxed to the quasi steady-state initial conditions. The boundary conditions at surface, bottom and coast for age are zero flux. On the open boundaries, age is relaxed to zero below 90 m, and to the time since the biological variables began varying in the top 90 m of the boundary.

Results

Analysis of vertical attenuation formulations

Before investigating the effect of alternate vertical attenuation formulations in the coupled physical–biological model, it is worth analysing the formulations for a range of cell sizes and wavelengths (Fig. 3). For this analysis, a biomass of phytoplankton of 1 mmol N m^{-3} is used, which is approximately the surface maximum obtained in the model in the region of interest. At the same time, a comparison is made with other formulations used in the literature.

Commonly, a nitrogen or chlorophyll-specific self-shading coefficient, k_c, is used to include the effect of phytoplankton

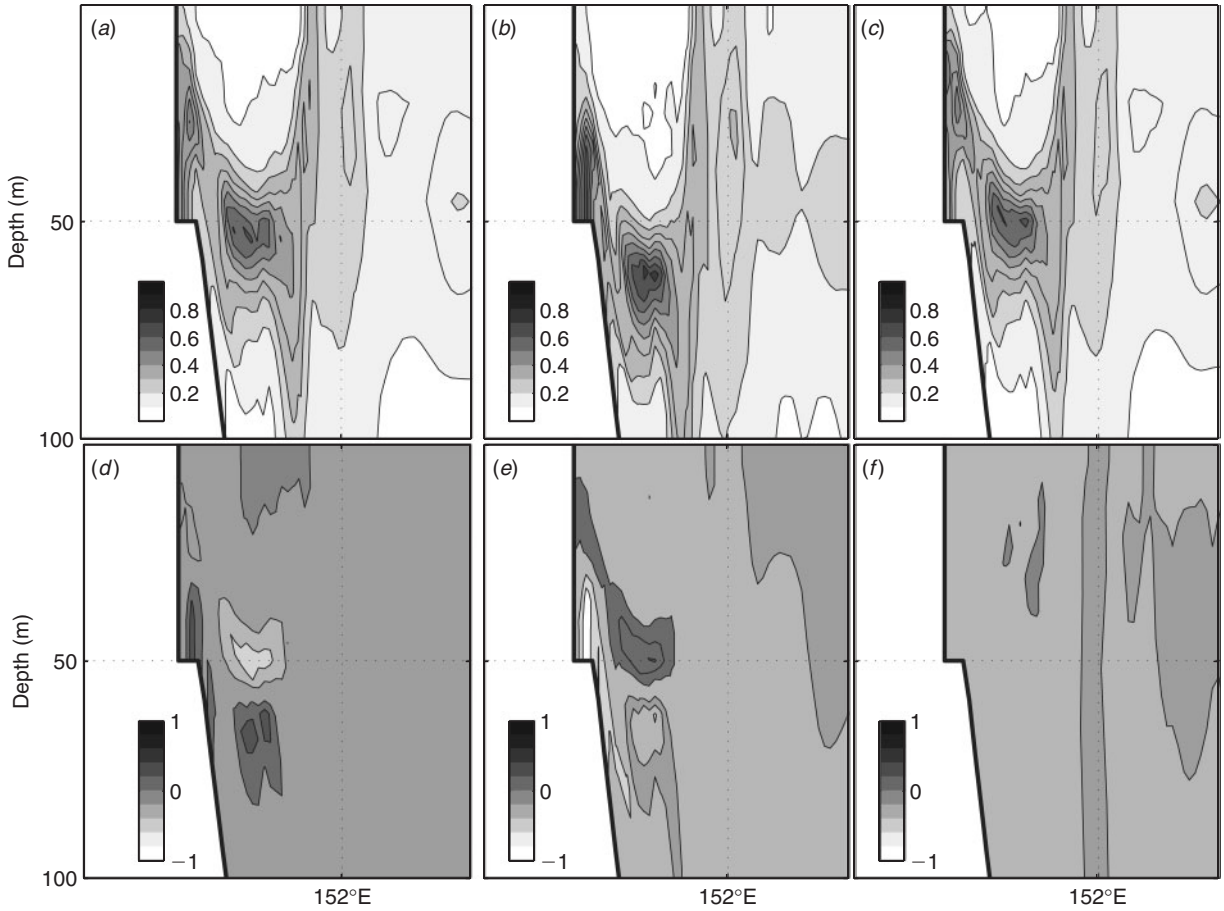

Fig. 5. Vertical slice of phytoplankton biomass (mmol N m^{-3}) along cross-shelf slice 145 (see Fig. 1) on Day 20.5 for (*a*) dissolved chlorophyll; (*b*) packaged chlorophyll without scattering; and (*c*) packaged chlorophyll with scattering, (*d*) the package effect [*b*–*a*]; (*e*) the scattering effect [*c*–*b*] and (*f*) the packaging and scattering effect [*c*–*a*].

on attenuation (Edwards *et al*. 2004). In Fig. 3*a*, the attenuation coefficient for self-shading formulation is calculated as $K = 0.04 + k_c P$, where $k_c = 0.03\ m^2$ (mmol N)$^{-1}$, and is independent of cell radius.

For spectrally averaged photosynthetically available radiation (300–700 nm), the package effect reduces the attenuation coefficient when compared with that of the dissolved chlorophyll formulation (Fig. 3*a*). The calculation of the attenuation coefficient using a self-shading parameter of 0.03 m^2 (mmol N)$^{-1}$ is equal to the packaging formulation at a cell radius of ~8 μm (intersection of lines in Fig. 3*a*). That is, the choice of 0.03 m^2 (mmol N)$^{-1}$ implicitly resolves the packaging effect at a radius of ~8 μm. At radii smaller than 8 μm, a choice of 0.03 m^2 (mmol N)$^{-1}$ underestimates the attenuation coefficient when compared with the packaging formulation.

Scattering increases attenuation from that of the packaging case without scattering. At a phytoplankton biomass of 1 mmol N m^{-3}, this results in greater vertical attenuation than the empirical formulation for all cell sizes. Morel (1988) used observations to propose an alternate empirical formulation of the vertical attenuation coefficient, $K = 0.027 + 0.0518\mathrm{Chl}^{0.428}$, which captures the varying attenuation with chlorophyll concentration. To compare with other formulations in Fig. 3*a*, an equivalent cell radius is calculated given a phytoplankton biomass of 1 mmol N m^{-3} and using the cell radius to chlorophyll relationship of Finkel (2001). At a phytoplankton biomass of 1 mmol N m^{-3}, the packaging and scattering formulation has a similar vertical attenuation coefficient to the Morel formulation, with the closest correspondence at a cell radius of ~15 μm.

Fig. 3*b*–*d* gives the vertical attenuation coefficient calculated using the alternate vertical attenuation formulations used in this paper for a range of cell sizes and wavelengths at a phytoplankton biomass of 1 mmol N m^{-3}. For all formulations, the attenuation coefficient is highest at 420 nm and lowest at 550 nm, coinciding with the absorbance maximum and minimum of chlorophyll (Hoepffner and Sathyendranath 1991). Packaging has the greatest fractional decrease in absorption at 420 nm [$\overline{naA_\lambda}/(\gamma_\lambda nCV) = 0.6$] and the least fractional decrease at 550 nm [$\overline{naA_\lambda}/(\gamma_\lambda nCV) = 0.99$] (Fig. 3*e*).

Effect of packaging and scattering on the spectra shape

Previous studies (Duyens 1956; Kirk 1976) have demonstrated that packaging of pigment within cells flattens the spectrum of light. The absorbing components of clear water and

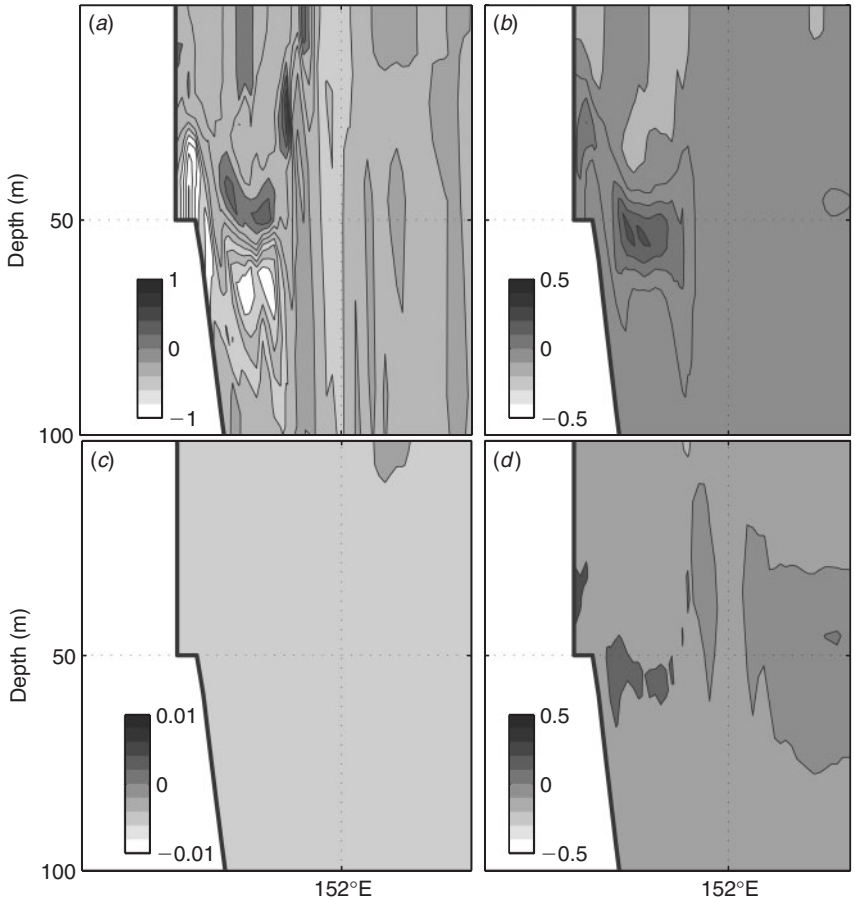

Fig. 6. Vertical slice of along cross-shelf slice 145 (see Fig. 1) on Day 20.5 for changes due to the package effect of (*a*) dissolved inorganic nitrogen (mmol N m^{-3}); (*b*) zooplankton (mmol N m^{-3}); (*c*) reserves of nitrogen, R_N/R_N^{max} and (*d*) reserves of energy R_I/R_I^{max}.

phytoplankton for a site off Port Stephens (Fig. 1) are given for dissolved chlorophyll (Fig. 4*a*) and for packaged chlorophyll (Fig. 4*c*). At this location, the vertical distributions of phytoplankton biomass for the three cases are relatively similar (inserts of Fig. 4*b*, *d*, *f*). The absorption by dissolved chlorophyll is twice the absorption of packaged chlorophyll at the peak absorbance (420 nm) (compare Fig. 4*a* and 4*c*). At the absorbance minimum, the absorption rates are similar. Packaged pigment has a more spectrally flat vertical attenuation coefficient, and, as a result, downwelling light shows a flatter spectrum (compare Fig. 4*b* and 4*d* at 10 m depth).

The effect of scattering is to increase vertical attenuation. The additional attenuation due to scattering is a function of the ratio of the scattering coefficient, $b_{T,\lambda}$, and the total absorbance, $k_\lambda + n\overline{aA_\lambda}$ (Eqn 7). The component of scattering as a result of phytoplankton is assumed to be constant for all wavelengths, whereas the component due to clear water scatters more strongly at shorter wavelengths (Fig. 2*e*). At the concentration of phytoplankton on the vertical profile off Port Stephens, the influence of scattering is significant between 340 and 500 nm owing to scattering by clear water (Fig. 2*e*), and between 500 and 600 nm owing to weak absorption by clear water (Fig. 2*c*) and phytoplankton (Fig. 2*f*). Above 600 nm, absorption due to clear water is high (Fig. 2*c*) and scattering becomes a small term.

Since it is only solar radiation of less than 600 nm (containing 28% of the energy in the modelled surface radiation field) that has a significantly different profile between cases, the vertical profile of solar heating is similar between the three formulations. In contrast, the radiation less than 600 nm contains ~63% of the light available for photosynthesis. So it is expected there will be a larger change in biological compared with physical properties owing to packaging and scattering.

Effect of packaging and scattering on biological dynamics

The largest effect of the vertical attenuation formulation in the coupled physical–biological model is on the spatial distribution of phytoplankton biomass. The increased penetration of light due to packaging of pigment results in the development of a deeper, and more intense, deep phytoplankton maximum (Fig. 5*a*, *b*, *d*). This effect is evident both in shallow water near the coast and on the edge of the continental shelf. Scattering reduces the light penetration (Fig. 5*b*, *c*, *e*) resulting in a vertical profile similar, but not identical, to the dissolved chlorophyll case (Fig. 5*f*).

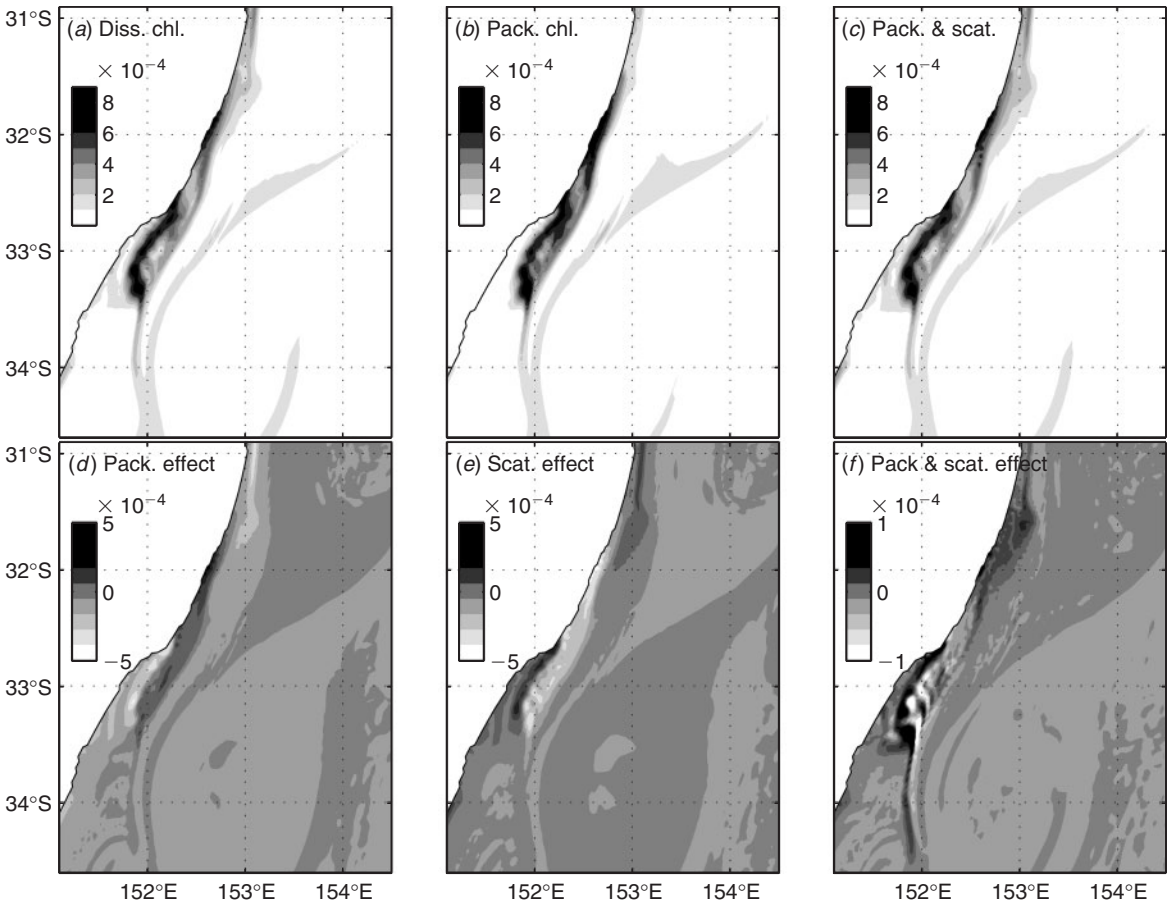

Fig. 7. Surface phytoplankton biomass (mol N m^{-3}) on Day 20.5 for (*a*) dissolved chlorophyll; (*b*) packaged chlorophyll without scattering; and (*c*) packaged chlorophyll with scattering; (*d*) the package effect [*b*–*a*]; (*e*) the scattering effect [*c*–*b*] and (*f*) the packaging and scattering effect [*c*–*a*].

The greater depth of the phytoplankton maximum in the packaged chlorophyll formulation of vertical attenuation alters the vertical distribution of the other biological state variables (Fig. 6). Dissolved inorganic nitrogen is depleted at a greater depth in the simulation with the packaged formulation (Fig. 6*a*). In the generally light-limited phytoplankton, reserves of energy are increased at depth (Fig. 6*d*), whereas reserves of nitrogen are virtually unchanged (Fig. 6*c*). The zooplankton field also moves downward, adjusting to the altered phytoplankton field (Fig. 6*b*).

The surface distribution of phytoplankton biomass is also altered south of Smoky Cape (Fig. 7). The formation of a deeper phytoplankton maximum, with associated nutrient depletion, results in upwelled water in the packaged formulation having a larger phytoplankton coastal bloom in the filament moving away from the coast at 32°S (Fig. 7*a*, *b*, *d*). Further evidence of this can be seen in Fig. 8*a* and *c*, where phytoplankton biomass is plotted against the age tracer (Eqn 1). The packaged chlorophyll formulation (Fig. 8*c*) has a chlorophyll peak that is slightly younger, and shorter lived, than the dissolved case. The relationship between age and zooplankton fields is also altered (Fig. 8*b* and *d*). In the packaged chlorophyll case, a larger, deeper chlorophyll maximum is being brought to the surface. Being both larger, and having a longer transit time, the biological response is more dynamic. The change in surface phytoplankton biomass is also associated with a small change in zooplankton biomass (not shown), with a filament of higher concentration zooplankton occurring on the western edge of the EAC soon after separation.

Effect of packaging and scattering on the physical–biological feedback

The previous studies have compared the effects of including (or excluding) the feedback between vertical distribution of plankton and physical properties (Edwards *et al*. 2001; Oschlies 2004). This section investigates the effect of three alternate forms of the vertical attenuation coefficient on the physical–biological feedback.

The effects of alternate vertical attenuation formulations on surface temperature and currents are graphed for the surface in Fig. 9. Model simulations with an inert tracer (not shown) demonstrate that the package effect moves the on-shore edge of the warm core eddy shoreward. This can be seen in the filament of positive temperature anomaly in Fig. 9*d*. The time-dependent surface age field shows the package effect produces younger water on the inshore edge of the eddy (Fig. 10*d*). The younger, upwelled water is colder than surface water, resulting in two

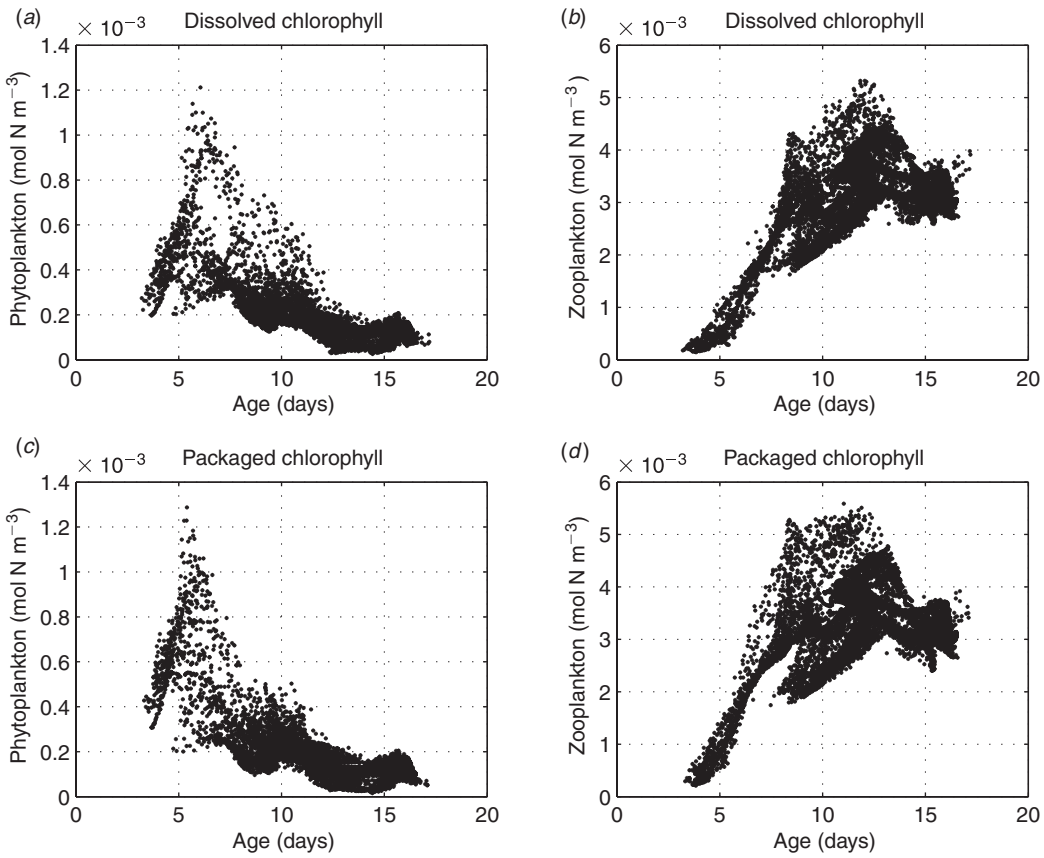

Fig. 8. Age versus phytoplankton biomass (left column) and zooplankton biomass (right column) for the dissolved chlorophyll formulation (top row) and package chlorophyll formulation (bottom row) (mol N m^{-3}) interpolated on to the 10 m depth level on Day 20.5.

pockets of cold water anomaly at 33°S and 34°S along 152°E longitude (Fig. 9*d*). Aside from these pronounced changes, the surface temperature field for the packaged case is slightly colder than the dissolved case (Fig. 9*d*) owing to increased light penetration resulting in deeper solar heating of the water column.

The package effect has a significant effect on surface currents (Fig. 9*d*). The most coherent effect is a broad region between 33.5–35°S and 152–153°E. In this region, the current anomaly is generally in the north-west direction of ~2–3 cm s^{-1} or ~2–3 km day^{-1}, and accounts for the shoreward movement of the warm core eddy. The movement of the eddy displaces the location of the greatest pressure gradient shoreward, resulting in the strongest current anomalies to the south along the temperature anomaly (Fig. 9*d*).

The scattering effect slightly warms the surface water, as shown by a generally warmer temperature anomaly (Fig. 9*e*). For much of the domain, the scattering effect temperature anomaly is the inversion of the packaged chlorophyll anomaly (compare Fig. 9*d* and 9*e*). Interestingly, the shoreward shift in the currents in the scattering case are not the reverse of the packaging case (Fig. 9*e*), and there is little change in vertical transport with the scattering effect, as shown by small age tracer anomalies (Fig. 10*e*).

The cause of the observed shift in the warm core eddy appears to be related to a stronger EAC. As noted above, the package effect will result in greater light penetration than the dissolved chlorophyll case. With a greater phytoplankton biomass inshore of the EAC, the penetration is greater inshore than offshore in the packaged case relative to the dissolved case. The nonlinearity of the equation of state determines that cooling warm water increases density more than cooling cold water (Mellor 1991). For the constant heat content approach used in the simulation, this results in an increase in density of the waters inshore of the EAC relative to offshore, creating a positive (in the offshore direction) elevation gradient. The elevation gradient drives a small acceleration of the EAC, with velocity anomalies of up to 5 cm s^{-1} seen north of Smoky Cape (not shown). This strengthened EAC appears to shift location of the warm core eddy.

Packaging and scattering effect for a 5 μm phytoplankton cell

Simulations with the dissolved chlorophyll and the packaged chlorophyll with scattering have been re-run with a 5 μm phytoplankton cell. It is necessary to re-run the dissolved chlorophyll case because changing cell size alters a range of biological rates (Table 1). Scattering plays a larger role in the 5 μm simulation. Absorption resulting from phytoplankton decreases owing to a stronger packaging effect. Scattering, which is dependent on the concentration of chlorophyll rather than the number of

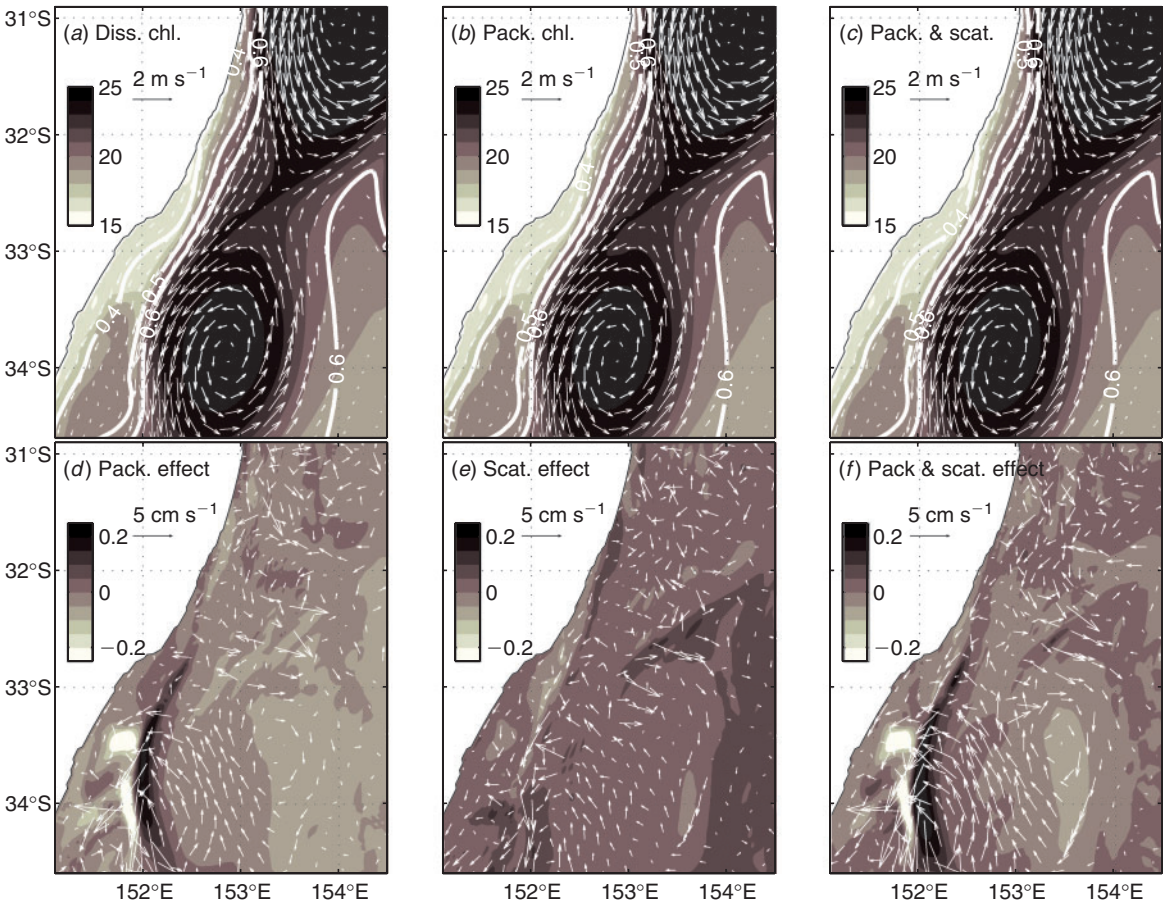

Fig. 9. Surface temperature (°C, shading), velocity (m s^{-1}, arrows) and elevation (m, line contours) on Day 20.5. For more details see Fig. 7.

cells (Eqn 7), is increased (owing to a greater phytoplankton biomass). As a result, the packaging and scattering effect for temperature and current (Fig. 11*e*) and the age tracer (Fig. 11*f*) appear reversed for a 5 μm phytoplankton cell compared with the 1-μm phytoplankton cell. This highlights the need to resolve the package and scattering effect, especially in size-based plankton models where the effect of cell size is being investigated.

Discussion and summary

Formulations of vertical attenuation

The comparison of the different formulations of the vertical attenuation coefficient demonstrates the importance of this term in coupled physical–biological models. Of course this importance has already been recognised in physical circulation models such as the Princeton Ocean Model (Blumberg and Mellor 1987) and the Modular Ocean Model (Pacanowski 1995) by the inclusion of a chlorophyll dependent vertical attenuation term. In these models, a constant self-shading parameter, k_c, is typically used. Fig. 3 demonstrates that the choice of k_c is important. It is interesting to consider how successful one parameter can be in implicitly representing the spectrally resolved dependence of vertical attenuation on absorption and scattering by phytoplankton of a range of sizes, shapes and pigment compositions.

Owing to the decrease in chlorophyll content with cell size (Eqn 17), the size-dependence of the package effect is much less than it would otherwise be. Fig. 3*e* gives the package effect, $\overline{naA_\lambda}/(\gamma_\lambda nCV)$, as a function of wavelength and cell size. Although the package effect, the fractional decrease in absorption, varies between 0.6 and 0.99 with wavelength, it is relatively independent of size. The reason for this can be seen in the phytoplankton cell opaqueness.

Opaqueness is the ratio of the light absorbed, $\overline{aA_\lambda}I$, to the total amount light intercepting the cell, $\pi r^2 I$ (Fig. 3*f*), which is almost independent of radius. The package effect arises because the volume fraction of phytoplankton cells has a different attenuation rate than if the pigment is suspended in the water. The constant opaqueness of cells over a range of cell sizes results in a volume fraction of phytoplankton with a similar attenuation coefficient relative to the dissolved pigment. As a result, the package effect is identical for cells of a range of sizes, but equal total volume and opaqueness.

It is possible to speculate at the level of the individual cell why this situation arises. As cellular chlorophyll concentration increases, the amount of light-absorbed asymptotes towards the limit of all light that falls on the projected area of the cell. At a particular wavelength, for a cell that is already absorbing 70% of the light reaching it, a doubling of chlorophyll (a biochemically

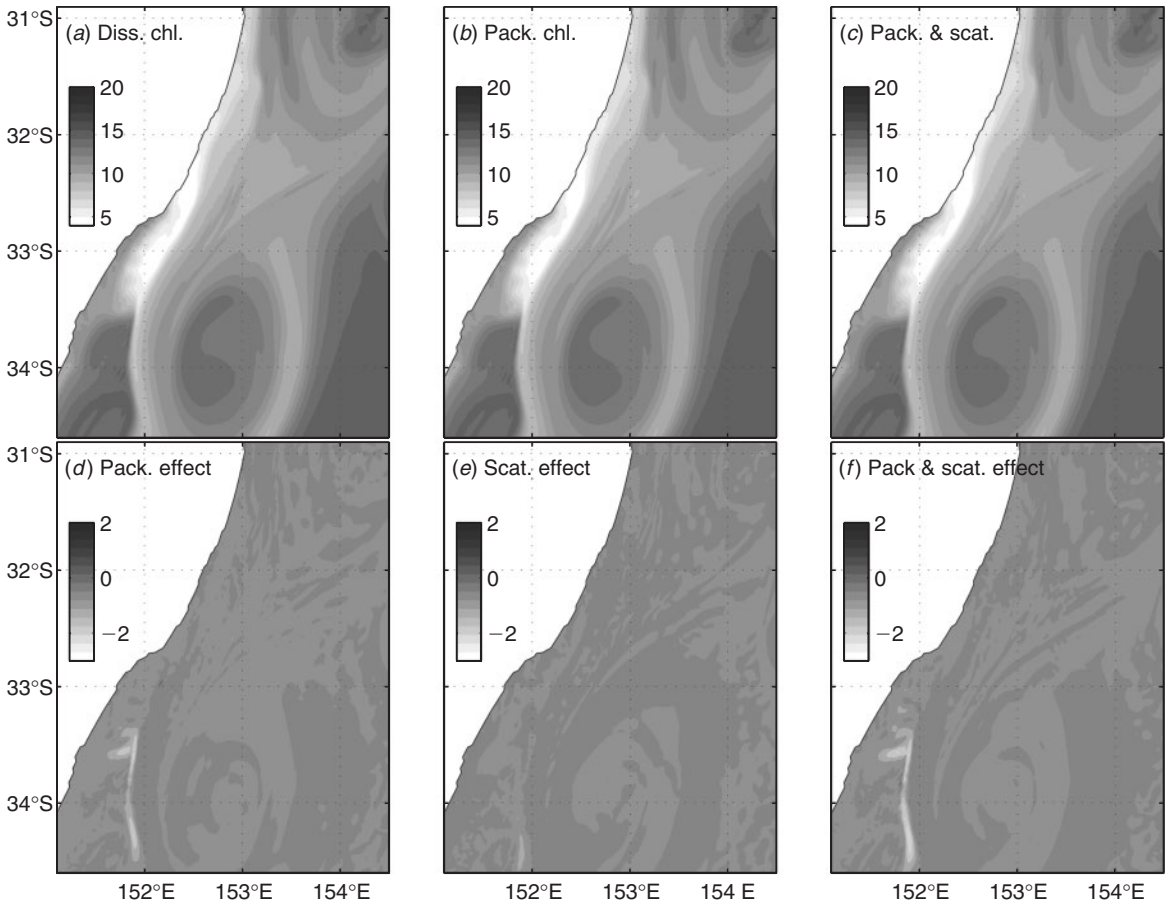

Fig. 10. Surface age (days) on Day 20.5. For more details see Fig. 7.

expensive molecule to produce) will increase the light absorbed to $\sim e^{2\log 0.3} = 90\%$. Given this diminishing return, it is not surprising that the opaqueness at 420 nm of all sizes of cells in the Finkel (2001) allometric relationship approach, but not too closely, 1.

The relative success of a one-parameter self-shading term has its origin in the relatively similar opaqueness of phytoplankton. Nonetheless, inaccuracies in a one-parameter formulation will be a result of effects such as the variations in absorbance with wavelength, variations in cell shape and pigment composition, deviations in chlorophyll concentration and nitrogen content from allometric relationships, as well as scattering. With the increasing number of size-structured plankton models being developed (Moloney and Field 1991; Gin *et al*. 1998; Armstrong 2003; Baird and Suthers 2007), the explicit inclusion of both the package effect and scattering should be considered.

Modelling the effects of packaging and scattering

Numerical models provide an opportunity to separate the impacts of packaging of pigments and scattering of light in a coupled physical–biological model. In the case of an $\sim$1 mmol N m^{-3} filament of 1 μm radius phytoplankton cells with an empirical scattering formulation following Kirk (1991), the effects of packaging and scattering on phytoplankton dynamics were broadly of equal magnitude and opposite direction. However, changes in spectral distribution of solar radiation and circulation changes suggest complex physical–biological feedbacks. The simulation with 5 μm radius phytoplankton cells illustrates how a change in parameter values leads to a changing balance between the scattering and packaging effects on vertical attenuation.

This study leaves many complexities of absorption and scattering unconsidered. Probably the most quantitatively significant aspects that are not considered are the variability of phytoplankton scattering properties with wavelength, and the effect of phytoplankton populations with a range of shapes, sizes and pigment compositions. To use a physical understanding to consider these processes will require a radiative transfer approach (Mishchenko *et al*. 2002), which is a well developed, but complex science.

In summary, through numerical experiments this study is able to isolate the effects of the packaging of pigments within cells and the scattering of light on physical–biological properties for an idealised scenario of conditions in the waters off south-east Australia. Packaging of pigment, through a reduction in the vertical attenuation coefficient, resulted in a deeper phytoplankton maximum. By altering the depth at which solar radiation heats the water column, packaging of pigment also shifted a developing warm core eddy onshore. Scattering, by increasing the attenuation coefficient, reduced the depth of the

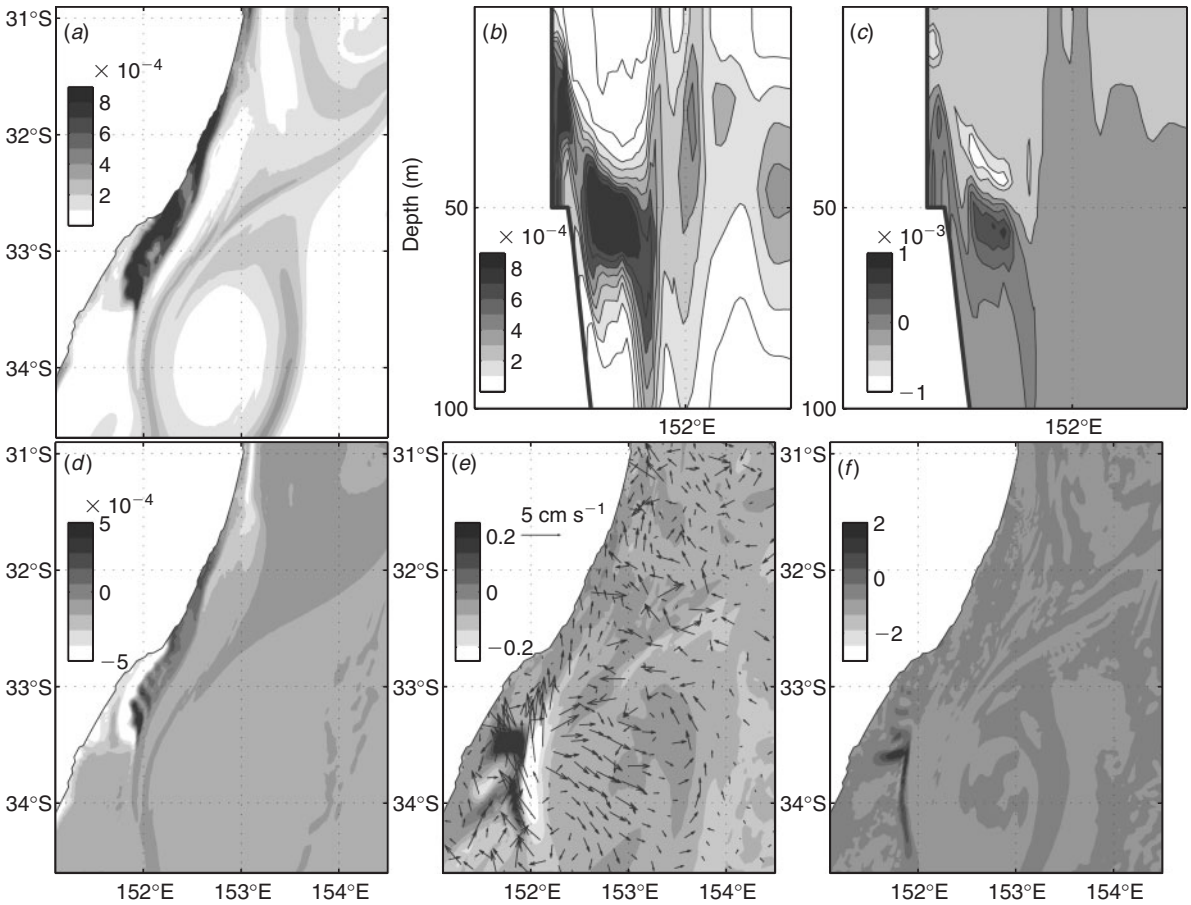

Fig. 11. The package and scattering effect for a 5 μm phytoplankton cell. (*a*) Surface phytoplankton biomass (compare with Fig. 7*c*); (*b*) vertical slice of phytoplankton biomass (compare with Fig. 5*c*); (*c*) package and scattering effect on phytoplankton biomass on a vertical slice (compare with Fig. 5*f*); (*d*) package and scattering effect on the surface phytoplankton biomass (compare with Fig. 7*f*); (*e*) package and scattering effect on surface temperature and velocity (compare with Fig. 9*f*); (*f*) package and scattering effect on surface age (compare with Fig. 10*f*).

deep phytoplankton maximum formation. The changes in model behaviour suggest that the modest cost of explicit representation of packaging of pigment and light scattering is worth considering in coupled physical–biological modelling studies.

Acknowledgements

This research was funded by ARC Discovery Projects DP0557618 held by MB and DP0208663 held by Jason Middleton (UNSW). Analysis of the model output for a lower resolution configuration was undertaken in partial fulfilment of Lujia Wu's Honours thesis at the UNSW. The use of the Australian Partnership for Advanced Computing (APAC) supercomputer, is gratefully acknowledged. We thank Alan Blumberg and George Mellor for the free availability of the Princeton Ocean Model (POM), and Patrick Marchesiello and Peter Oke for earlier work on the POM configuration for the waters off south-east Australia.

References

Armstrong, R. A. (2003). A hybrid spectral representation of phytoplankton growth and zooplankton response: the control rod model of planktonic interaction. *Deep-Sea Research. Part II, Topical Studies in Oceanography* **50**, 2895–2916. doi:10.1016/J.DSR2.2003.07.003

Atkins, P. W. (1994). 'Physical Chemistry,' 5th edn. (Oxford University Press: Oxford.)

Baird, M. E. (2003). Numerical approximations of the mean absorption cross-section of a variety of randomly oriented microalgal shapes. *Journal of Mathematical Biology* **47**, 325–336. doi:10.1007/S00285-003-0215-9

Baird, M. E., and Suthers, I. M. (2007). A size-resolved pelagic ecosystem model. *Ecological Modelling* **203**, 185–203. doi:10.1016/J. ECOLMODEL.2006.11.025

Baird, M. E., Oke, P. R., Suthers, I. M., and Middleton, J. H. (2004). A plankton population model with bio-mechanical descriptions of Biological processes in an idealised 2-D ocean basin. *Journal of Marine Systems* **50**, 199–222. doi:10.1016/J.JMARSYS.2004.02.002

Baird, M. E., Timko, P. G., Suthers, I. M., and Middleton, J. H. (2006*a*). Coupled physical–biological modelling study of the East Australian Current with idealised wind forcing. Part I: Biological model intercomparison. *Journal of Marine Systems* **59**, 249–270. doi:10.1016/J.JMARSYS.2005.09.005

Baird, M. E., Timko, P. G., Suthers, I. M., and Middleton, J. H. (2006*b*). Coupled physical–biological modelling study of the East Australian Current with idealised wind forcing: Part II: Biological dynamical analysis. *Journal of Marine Systems* **59**, 271–291. doi:10.1016/J.JMARSYS.2005.09.006

Blumberg, A. F., and Mellor, G. L. (1987). A description of a three-dimensional coastal ocean circulation model. In 'Three-dimensional Coastal Ocean Models'. (Ed. N. Heaps.) pp. 1–15. (American Geophysical Union: Washington, DC.)

Brock, T. D. (1981). Calculating solar radiation for ecological studies. *Ecological Modelling* **14**, 1–19. doi:10.1016/0304-3800(81)90011-9

Chu, P. C., and Fan, C. (2003). Hydrostatic correction for sigma coordinate ocean models. *Journal of Geophysical Research* **108**(C6), 3206. doi:10.1029/2002JC001668

Craig, P. D., and Banner, M. L. (1994). Modeling wave-enhanced turbulence in the ocean surface layer. *Journal of Physical Oceanography* **24**, 2546–2559. doi:10.1175/1520-0485(1994)024<2546:MWETIT>2.0.CO;2

Duyens, L. N. M. (1956). The flattening of the absorption spectra of suspensions as compared to that of solutions. *Biochimica et Biophysica Acta* **19**, 1–12. doi:10.1016/0006-3002(56)90380-8

Edwards, A. M., Platt, T., and Wright, D. G. (2001). Biologically-induced circulations at fronts. *Journal of Geophysical Research* **106**(C4), 7081–7096. doi:10.1029/2000JC000332

Edwards, A. M., Platt, T., and Wright, D. G. (2004). Biological heating effect of a band of phytoplankton. *Journal of Marine Systems* **49**, 89–103. doi:10.1016/J.JMARSYS.2003.05.011

England, M. H. (1995). The age of water and ventilation time scales in a global ocean model. *Journal of Physical Oceanography* **25**, 2756–2777. doi:10.1175/1520-0485(1995)025<2756:TAOWAV>2.0.CO;2

Fasham, M. J. R., Ducklow, H. W., and McKelvie, S. M. (1990). A nitrogen-based model of plankton dynamics in the oceanic mixed layer. *Journal of Marine Research* **48**, 591–639.

Finkel, Z. V. (2001). Light absorption and size scaling of light-limited metabolism in marine diatoms. *Limnology and Oceanography* **46**, 86–94.

Gildor, H., and Naik, N. H. (2005). Evaluating the effect of interannual variations of surface chlorophyll on upper ocean temperature. *Journal of Geophysical Research* **110**, C07012. doi:10.1029/2004JC002779

Gin, K. Y. H., Guo, J., and Cheong, H.-F. (1998). A size-based ecosystem model for pelagic waters. *Ecological Modelling* **112**, 53–72. doi:10.1016/S0304-3800(98)00126-4

Gregg, W. W., and Carder, K. L. (1990). A simple spectral solar irradiance model for cloudless maritime atmospheres. *Limnology and Oceanography* **35**, 1657–1675.

Hall, T. M., and Haine, T. W. N. (2002). On ocean transport diagnostics: the idealized age tracer and the age spectrum. *Journal of Physical Oceanography* **32**, 1987–1991. doi:10.1175/1520-0485(2002)032<1987:OOTDTI>2.0.CO;2

Hoepffner, N., and Sathyendranath, S. (1991). Effect of pigment composition on absorption properties of phytoplankton. *Marine Ecology Progress Series* **73**, 11–23. doi:10.3354/MEPS073011

Hofmann, M., Wolf-Gladrow, D. A., Takahashi, T., Sutherland, S. C., Six, K. D., and Maier-Reimer, E. (2000). Stable carbon isotope distribution of particulate organic matter in the ocean: a model study. *Marine Chemistry* **72**, 131–150. doi:10.1016/S0304-4203(00)00078-5

Kirk, J. T. O. (1975). A theoretical analysis of the contribution of algal cells to the attenuation of light within natural waters. II. Spherical cells. *The New Phytologist* **75**, 21–36. doi:10.1111/J.1469-8137.1975.TB01367.X

Kirk, J. T. O. (1976). A theoretical analysis of the contribution of algal cells to the attenuation of light within natural waters. III. Cylindrical and spheroidal cells. *The New Phytologist* **77**, 341–358. doi:10.1111/J.1469-8137.1976.TB01524.X

Kirk, J. T. O. (1981). A Monte Carlo study of the nature of the underwater light field in, and the relationship between optical properties of, turbid yellow waters. *Australian Journal of Marine and Freshwater Research* **32**, 517–532. doi:10.1071/MF9810517

Kirk, J. T. O. (1991). Volume scattering function, average cosines, and the underwater light field. *Limnology and Oceanography* **36**, 455–467.

Kirk, J. T. O. (1994). 'Light and Photosynthesis in Aquatic Ecosystems,' 2nd edn. (Cambridge University Press: Cambridge.)

Kistler, R., Kalnay, E., Collins, W., Saha, S., White, G., *et al.* (2001). The NCEP-NCAR 50-year reanalysis: monthly means CD-rom and documentation. *Bulletin of the American Meteorological Society* **82**, 247–267. doi:10.1175/1520-0477(2001)082<0247:TNNYRM>2.3.CO;2

Koller, L. R. (1965). 'Ultraviolet Radiation,' 2nd edn. (John Wiley and Sons, Inc.: New York.)

Lewis, M. R., Cullen, J. J., and Platt, T. (1983). Phytoplankton and thermal structure in the upper ocean: consequences of nonuniformity in chlorophyll profile. *Journal of Geophysical Research* **88**, 2565–2570.

Marchesiello, P., McWilliams, J. C., and Shchepetkin, A. (2001). Open boundary conditions for long-term integration of regional oceanic models. *Ocean Modelling* **3**, 1–20. doi:10.1016/S1463-5003(00)00013-5

Mellor, G. L. (1991). An equation of state for numerical models of oceans and estuaries. *Journal of Atmospheric and Oceanic Technology* **8**, 609–611. doi:10.1175/1520-0426(1991)008<0609:AEOSFN>2.0.CO;2

Mishchenko, M. I., Travis, L. D., and Lacis, A. A. (2002). 'Scattering, Absorption and Emission of Light by Small Particles.' (Cambridge University Press: Cambridge.)

Moloney, C. L., and Field, J. G. (1991). The size-based dynamics of plankton food webs. I. A simulation model of carbon and nitrogen flows. *Journal of Plankton Research* **13**, 1003–1038. doi:10.1093/PLANKT/13.5.1003

Morel, A. (1988). Optical modelling of the upper ocean in relation to its biogenous matter content (Case I waters). *Journal of Geophysical Research* **93**, 10 749–10 768.

Oke, P. R., and Middleton, J. H. (2001). Nutrient enrichment off Port Stephens: the role of the East Australian Current. *Continental Shelf Research* **21**, 587–606. doi:10.1016/S0278-4343(00)00127-8

Oschlies, A. (2004). Feedbacks of biotically induced radiative heating on upper-ocean heat budget, circulation, and biological production in a coupled ecosystem-circulation model. *Journal of Geophysical Research* **109**, C12031. doi:10.1029/2004JC002430

Pacanowski, R. (1995). MOM2 Documentation User's Guide and Reference Manual: GFDL Ocean Group Technical Report. Geophysical Fluid Dynamics Laboratory (GFDL), National Oceanic and Atmospheric Administration, Princeton, NJ.

Pegau, S., Zanefeld, J., Mitchell, B., Mueller, J., Kahru, M., Wieland, J., and Stramska, M. (2003). Ocean Optics Protocols for Satellite Ocean Color Sensor Validation, Revision 4, Volume IV: Inherent Optical Properties: Instruments, Characterization, Field Measurements and Data Analysis Protocols. NASA/TM-2003-211621/Rev4-Vol. IV. Technical Report. (Eds J. L. Mueller, G. S. Fargion and C. R. McClain.) NASA Goddard Space Flight Center, Greenbelt, MD.

Redfield, A. C., Ketchum, B. H., and Richards, F. A. (1963). The influence of organisms on the composition of sea-water. In 'The Sea', 2nd edn. (Ed. N. Hill.) pp. 26–77. (Wiley: New York.)

Roughan, M., and Middleton, J. H. (2002). A comparison of observed upwelling mechanisms off the east coast of Australia. *Continental Shelf Research* **22**, 2551–2572. doi:10.1016/S0278-4343(02)00101-2

Sathyendranath, S., Prieur, L., and Morel, A. (1989). A three-component model of ocean colour and its application to remote sensing of phytoplankton pigments in coastal waters. *International Journal of Remote Sensing* **10**, 1373–1394. doi:10.1080/01431168908903974

Smith, R. C., and Baker, K. S. (1981). Optical properties of the clearest natural waters. *Applied Optics* **20**, 177–184.

Stramska, M., and Dickey, T. D. (1993). Phytoplakton bloom and the vertical thermal structure of the upper ocean. *Journal of Marine Research* **51**, 819–842. doi:10.1357/0022240933223918

Manuscript received 18 June 2007, accepted 14 September 2007